Published in final edited form as:
Aerosol Sci Technol. 2011 January 1; 45(7): 884–899. doi:10.1080/02786826.2011.566592.

Numerical Model to Characterize the Size Increase of Combination Drug and Hygroscopic Excipient Nanoparticle Aerosols

P. Worth Longest[1,2,*] and **Michael Hindle**[2]

[1] Department of Mechanical Engineering, Virginia Commonwealth University, Richmond, VA

[2] Department of Pharmaceutics, Virginia Commonwealth University, Richmond, VA

Abstract

Enhanced excipient growth is a newly proposed respiratory delivery strategy in which submicrometer or nanometer particles composed of a drug and hygroscopic excipient are delivered to the airways in order to minimize extrathoracic depositional losses and maximize lung retention. The objective of this study was to develop a validated mathematical model of aerosol size increase for hygroscopic excipients and combination excipient-drug particles and to apply this model to characterize growth under typical respiratory conditions. Compared with *in vitro* experiments, the droplet growth model accurately predicted the size increase of single component and combination drug and excipient particles. For typical respiratory drug delivery conditions, the model showed that droplet size increase could be effectively correlated with the product of a newly defined hygroscopic parameter and initial volume fractions of the drug and excipient in the particle. A series of growth correlations was then developed that successively included the effects of initial drug and excipient mass loadings, initial aerosol size, and aerosol number concentration. Considering EEG delivery, large diameter growth ratios (2.1–4.6) were observed for a range of hygroscopic excipients combined with both hygroscopic and non-hygroscopic drugs. These diameter growth ratios were achieved at excipient mass loadings of 50% and below and at realistic aerosol number concentrations. The developed correlations were then used for specifying the appropriate initial mass loadings of engineered insulin nanoparticles in order to achieve a predetermined size increase while maximizing drug payload and minimizing the amount of hygroscopic excipient.

Keywords

Respiratory drug delivery; enhanced excipient growth (EEG); nanoaerosols; hygroscopic droplet growth; hygroscopic excipients; combination particles; engineered particles; *in vitro* experiments of aerosol growth; capillary aerosol generation; numerical simulations; targeted drug delivery

[*]Corresponding author: Dr. P. Worth Longest, PhD, Virginia Commonwealth University, 401 West Main Street, P.O. Box 843015, Richmond, VA 23284-3015, Phone: (804)-827-7023, Fax: (804)-827-7030, pwlongest@vcu.edu.
Dr. Michael Hindle, PhD, Virginia Commonwealth University, 410 N. 12th St., P.O. Box 980533, Richmond, VA 23284, Phone: (804)-828-6497, mhindle@vcu.edu

Author Disclosure Statement
No conflicts of interest exist.

INTRODUCTION

The low efficiencies at which current inhalers deliver drugs to the lungs are well known and arise primarily from high depositional losses in the device and extrathoracic airways. Current *in vivo* and *in vitro* studies indicate that characteristic mouth-throat (MT) depositional losses range from approximately 25–60% for HFA pressurized metered dose inhalers (MDIs) (Leach et al. 1998; Cheng et al. 2001; Zhang et al. 2007; Longest et al. 2008a; Hindle and Longest 2010) and from 50–70% for dry powder inhalers (DPIs) (Newman and Busse 2002; Zhang et al. 2007; Byron et al. 2010). Depositional losses also occur in the actuator and mouthpiece resulting in wasted medication (Longest et al. 2008a; Longest and Hindle 2009a), which is often ignored. Nebulizer systems can be used to deliver higher doses of inhaled medications, but have extrathoracic deposition and lung delivery efficiencies similar to MDIs and DPIs (Newman 2009). The use of mesh nebulizers allows for the generation of a relatively monodisperse aerosol on demand (Hardaker and Hatley 2010). Synchronization of a mesh nebulizer with the inhalation waveform was recently reported to produce lung deliveries of approximately 60–70% (Nikander et al. 2010). Next-generation softmist inhalers such as capillary aerosol generation (CAG) and the Respimat inhaler are also reported to reduce MT deposition to approximately 20% (Pitcairn et al. 2005; Longest et al. 2008b). However, device deposition may remain high for softmist systems (Longest and Hindle 2009a). While improvements in the delivery of inhaled aerosols have been observed, mouth-throat and device depositional losses, and the associated high variability of drug delivery to the lungs (Borgstrom et al. 2006), may still be too large for the practical implementation of many envisioned next-generation inhaled medicines with narrow therapeutic windows that require precise dosing and targeted regional lung deposition.

To improve the lung delivery of inhaled medicines, the concept of controlled size increase was recently introduced (Longest et al. 2010). In this approach, the aerosol is delivered with an initially small (submicrometer or nanometer) size to significantly reduce device and extrathoracic depositional losses at all practical flow rates. Increasing the aerosol size as it enters the lungs is then used to ensure lung retention and to potentially target the site of delivery within the airways. One previously reported method to increase aerosol size post-inhalation is enhanced condensational growth (ECG). In this approach, a submicrometer aerosol is delivered in combination with saturated or supersaturated air a few degrees above body temperature. Cooling of the humidity stream, by mixing with the aerosol or interactions with the airway walls, produces a supersaturated environment in the airways and results in subsequent aerosol growth. Longest et al. (2010) introduced the ECG process and showed that initially submicrometer pharmaceutical aerosols could increase in size to a target range of approximately 2–3 μm using temperatures appropriate for respiratory drug delivery. Longest and Hindle (2010) developed and validated a computational fluid dynamics (CFD) model of aerosol size increase during the ECG process. Hindle and Longest (2010) evaluated ECG aerosol delivery in a realistic model of the MT and upper tracheobronchial (TB) region extending to the fifth respiratory bifurcation. Experimental results showed that MT drug deposition was minimal (~1%) and that TB deposition increased with ECG by an order of magnitude, which indicated significant aerosol growth. A primary advantage of the ECG approach is that it can be applied with any conventional pharmaceutical aerosol delivered in the submicrometer range. However, this method does require the generation and delivery of a saturated or supersaturated warm airstream.

An alternative approach that may also increase the size of an aerosol after inhalation is the inclusion of hygroscopic excipients. Longest and Hindle (2009b) have recently proposed the concept of enhanced excipient growth (EEG), in which hygroscopic excipients are included with medicines as combination submicrometer or nanometer particles or droplets. As a result

of the initially small aerosol size, very low extrathoracic deposition can be achieved. The natural water vapor in the respiratory airways is then used in combination with the hygroscopic excipient to increase the size of the particles and thereby enhanced deposition. The relative humidity (RH) of the airways under normal inhalation conditions reaches the wall value of 99.5% around the third or fourth bifurcation (Zhang et al. 2006b). As a result, the submicrometer aerosol is expected to penetrate deep within the TB tree before significant growth occurs. Due to the absence of an external source of water vapor, coupling between the aerosol phase and RH of the airways is expected to be stronger than with ECG delivery. However, a primary advantage of this approach is that an external water vapor source is not needed. With this method, engineered combination particles can be delivered with existing inhalers capable of producing a submicrometer or nanometer aerosol. Specifically, solution based MDIs, active DPIs, and new softmist inhalers may be modified to generate the initially nanometer-sized aerosol. However, the amount and type of hygroscopic excipients required to produce a specific size increase in the respiratory airways is not known.

Previous studies have considered the hygroscopic growth of single component drug and environmental aerosols in the respiratory airways. Ferron et al. (1989) showed that salt particles could increase in size by a factor of approximately 4. Drug aerosols were also shown to increase in size, but growth was variable based on the material considered and occurred to a lesser extent than with conventional salts. Finlay and Stapleton (1995) and Finlay (1998) showed that two-way coupling significantly limits the size increase of conventional aerosols greater than approximately 3 μm. Two-way coupling refers to the effect of the droplet phase on the surrounding air (as well as the effect of the surrounding air on the droplets). Other studies have developed models for the growth of multicomponent respiratory aerosols (Robinson and Yu 1998; Longest and Kleinstreuer 2005; Longest and Xi 2008); however, two-way coupling effects were not considered. Recent whole-lung deposition simulations have indicated that both hygroscopic growth and two-way coupling can significantly impact deposition (Broday and Georgopoulous 2001; Varghese and Gangamma 2009). Zhang et al. (2006a) used a CFD model to show that sodium chloride mass fractions of approximately 10% and greater were required to influence the deposition of hypertonic micrometer aerosols.

A number of factors will influence the hygroscopic growth of combination particles in the respiratory tract. These factors can be categorized as (i) hygroscopicity of the excipient and drug, (ii) properties of the engineered particle, (iii) characteristics of the aerosol, and (iv) respiratory parameters. Hygroscopic growth occurs because a dissolved material reduces the water vapor pressure on the surface of the droplet below the value of the surrounding air. Factors affecting the droplet surface vapor pressure, thereby defining the hygroscopicity of the excipient or drug, include the solubility, dissociation, molecular weight, and density of the dissolved material. Properties of the engineered particles or droplets affecting the final size include the initial size, drug and excipient selected, initial mass fractions of the drug and excipient, and liquid or solid forms of the excipients. The primary characteristic of the aerosol affecting growth is the number concentration, which controls the degree of two-way coupling and can limit the final size achieved. Considering respiratory parameters, final size will be controlled by the period of exposure and thermodynamic conditions in the distal respiratory airways (i.e., T = 37 °C and RH = 99.5%).

While the hygroscopic growth of respiratory aerosols has been previously considered, a number of factors related to the size increase of aerosols during EEG have not been assessed. Previous studies have not reported the hygroscopic growth of multicomponent aerosols including the effects of two-way coupling. Finlay and Stapleton (1995) and Finlay (1998) showed that the hygroscopic growth of conventional pharmaceutical aerosols could

typically be neglected for sizes greater than approximately 3 μm. However, smaller aerosols and the inclusion of hygroscopic excipients may result in a greater impact on deposition. Furthermore, the hygroscopic effects together with the effects of particle and aerosol properties on droplet growth and final size in the respiratory airways are not well understood. For example, it is not known if doubling the mass fraction of the hygroscopic excipient in a combination particle is necessary to double the final size obtained. As a result, both a validated numerical model and a characterization study are needed to assess expected aerosol behavior during EEG delivery.

The objective of this study is to develop a validated mathematical model of aerosol size increase for hygroscopic excipients and combination drug-excipient particles and to apply this model to characterize growth under typical respiratory conditions. The model will include full coupling between the aerosol and vapor phase and between the air phase and respiratory walls. The validation study will be performed by comparing model predictions to experimentally measured values of aerosol growth for both drug and drug-excipient combination particles after a specific exposure period. The model will then be applied to determine the effects of hygroscopic characteristics, particle parameters, and aerosol properties on growth for typical respiratory exposure conditions. Functional relationships will be sought to characterize the complex interconnections of the relevant variables and thereby dramatically simplify the growth predictions. These functional relationships will help to identify the parameters most responsible for aerosol size increase. Moreover, these relationships can be used to engineer particle characteristics to achieve a desired level of size change and thereby target deposition within specific regions of the airways.

METHODS

Experimental Design

For experimental validation of the numerical model, a test system was constructed as shown in Fig. 1. Submicrometer single component and combination particles were formed using a capillary aerosol generator (CAG). The capillary aerosol generation system is described and considered in detail by the previous studies of Hindle et al. (1998) and Longest et al. (2007). In the current study, the solution vehicle was a mixture of 50% water and 50% ethanol by weight to dissolve both hydrophilic and hydrophobic drugs in solution formulations. The formulations were heated and pumped through the CAG at a flow rate of 10 mg/s to form the spray aerosol. Drug only and combination drug-excipient particles were created experimentally using albuterol sulfate (AS), budesonide (BD), and sodium chloride (NaCl). Specifically, single component drug particles were formed for AS and BD using a 0.2% w/v AS solution and a 0.15% w/v BD solution, respectively. Combination drug-excipient particles were generated using a 0.1% AS - 0.1% NaCl w/v solution and a 0.1% BD - 0.1% NaCl w/v solution. The spray aerosol was allowed to dry into solid particles by passage through a 52 cm length of dry tubing (Fig. 1). As described by Longest et al. (2007), the CAG delivers a bolus of warm vapor and droplets over a time period of approximately 2 s. Walls of the initially dry tube were at ambient temperature conditions. As the warm bolus travels through the tubing, condensation onto the wall surface occurs resulting in removal of the water vapor from the air phase and drying of the aerosol.

To produce aerosol growth, the aerosol stream was combined with humidified air at T = 25 °C and RH = 99% sampled from an environmental cabinet (Espec, Hudsonville, MI). The combined aerosol mixture had a flow rate of approximately 30 ± 2 L/min and was passed through a 26 cm length of tubing (the growth zone) with a diameter of 2 cm (Fig. 1). This length was selected to provide a residence time of approximately 0.2 s, which is consistent with the time required for an orally inhaled pharmaceutical aerosol to reach the main bifurcation of the lungs under standard inhalation conditions. Walls of the growth section

were pre-wetted to simulate the wet walled conditions of the respiratory tract, which stimulates aerosol growth. The growth tube was not heated and was exposed to 24 °C room temperature air for this initial validation experiment.

The temperature and humidity of the humidified air and the temperature of the aerosol mixture stream at the inlet to the condensational growth tube were measured in separate experiments. These measurements were performed using the Humicap Handheld Meter (HMP75B, Vaisala, Helsinki, Finland) positioned at the mid-plane of the tubing and a sheathed Type K thermocouple (Omega Engineering Corp., Stamford, CT) positioned at the mid-plane of the tubing. The Humicap Handheld Meter has a stated temperature accuracy of ±0.2 °C (at 20 °C) and ±0.25 °C (at 40 °C). It has a RH accuracy of ±1.7% (at 20 °C) and ±1.8% (at 40 °C) between 90–100 % RH. The probe was factory calibrated using traceable standards and supplied with a NIST calibration certificate. The probe was housed in a plastic filter and incorporated a sensor pre-heater which was employed to prevent condensation during equilibration prior to measurement.

In separate experiments, the initial dry particle size of the aerosol and the final size after passage through the growth tube were determined. Sizing was performed using an 8 stage MOUDI (MSP Corp, Shoreview, MN) operated at 30 ± 2 L/min and maintained at 25 °C by placing it in the environmental chamber. In order to determine the initial dry particle size, the impactor was connected at the exit of the drying tube as shown in Fig 1 (the growth tube was not present for these experiments). To maintain operation of the impactor at 30 L/min without increasing the airflow around the CAG, additional air was drawn through the humidity line with a temperature and RH of 25 °C and 46%, respectively. To determine the aerosol size after exposure to 99% RH, the MOUDI was connected to the outlet of the growth tube, as shown in Fig. 1. Air entering the humidified air inlet during the growth experiments was at 25 °C and 99% RH, as described above. For both the initial and final particle size distributions, following aerosol generation, washings using appropriate volumes (5–25ml) were collected from the impaction plates to determine the drug deposition. A 1:1 admixture of methanol and deionized water was used, and the solutions were then assayed using validated HPLC-UV methods for AS and BD. The mass of drug on each impaction plate was determined and used to calculate both the initial and final aerodynamic particle size distributions of the drug and combination aerosols. Aerosol droplet size distributions were reported as mass distribution recovered from the impactor. The mass median aerodynamic diameter (MMAD) was defined as the particle size at the 50th percentile on a cumulative percent mass undersize distribution (D50) using linear interpolation. Four replicates of each experiment were performed.

The drug:excipient ratio in the combination particles was determined by accurately weighing a mass of dry combination particles and then assaying it to determine the drug content in a set of separate experiments. The mass of excipient in the particle was determined by difference (mass of excipient = mass of particle − mass of drug). This was then used to calculate the mean (SD) drug:excipient ratio (n=10).

To calculate the effects of solutes on the surface vapor pressure of aqueous solutions, the water activity of drug and excipient solutions was determined as a function of mass fraction. Water activity was calculated by measuring the relative humidity of the air surrounding the sample after reaching equilibrium in a sealed container. A chilled mirror dew point hygrometer (General Electric Co., Fairfield, CT) was used to measure the ambient air temperature and the dew point for solutions containing either drug or hygroscopic excipient at a series of different mass fractions (mf) depending on the compound (citric acid: mf = 0.092–0.545, propylene glycol: mf = 0.5–0.615, albuterol sulfate: mf = 0.032–0.2).

Numerical Model and Solution

The numerical model considers a group of monodisperse droplets with number concentration n_{part} flowing in the *in vitro* system or respiratory airways. Well mixed conditions are assumed at each time level, which is equivalent to considering radially constant conditions at each depth of penetration into the respiratory model, i.e., a 1-D approach. Heat and mass transfer are considered between the droplets and air phase and between the air and wall. The interconnected first order non-linear differential equations governing the droplet temperature (T_d), droplet radius (r_d), air temperature (T_{air}), and water vapor mass fraction in the air ($Y_{v,air}$) are

$$\frac{dT_d}{dt}=\frac{3}{\rho_d C p_d r_d}(-\bar{q}_d - L_v \bar{n}_d) \tag{1}$$

$$\frac{dr_d}{dt}=\frac{-\bar{n}_d}{\rho_w} \tag{2}$$

$$\frac{dT_{air}}{dt}=\frac{4\pi r_d^2}{\rho_{air} C p_{air}} \bar{q}_d n_{part} + \frac{\bar{q}_{wall}}{\rho_{air} C p_{air}} \frac{4}{D_{tube}} \tag{3}$$

$$\frac{dY_{v,air}}{dt}=\frac{4\pi r_d^2}{\rho_{air}} \bar{n}_d n_{part} + \frac{\bar{n}_{wall}}{\rho_{air}} \frac{4}{D_{tube}} \tag{4}$$

In these expressions, ρ and Cp are the densities and specific heats of the droplet (d), air, and water (w). The first equation describes droplet temperature change based on convective ($\bar{q}_d$) and evaporating ($L_v \bar{n}_d$) heat fluxes at the droplet surface. In this expression, L_v represents the latent heat of water vaporization and $\bar{n}_d$ is the evaporating or condensing mass flux at the surface. Overbars on the flux values indicate area-averages taken over the droplet surface, based on the rapid mixing assumption (Longest and Kleinstreuer 2005). Equation (2) describes the rate of droplet size change as a function of surface mass flux. The third equation describes the well mixed air temperature at each time, which is controlled by the convective flux from the droplet and the heat flux from the walls ($\bar{q}_{wall}$) for a tube with a characteristic diameter D_{tube}. The mass fraction of water vapor in the air ($Y_{v,air}$) is influenced by the mass gained or lost at the droplet surface and the wall mass flux ($\bar{n}_{wall}$).

The flux components at the droplet surface in Eqs. (1–4) can be defined as

$$\bar{q}_d=\frac{Nu \kappa_{air} C_T}{2 r_d}(T_d - T_{air}) \tag{5}$$

$$\bar{n}_d=\rho_{air} \frac{Sh \tilde{D}_v C_M}{2 r_d} \frac{Y_{v,surf} - Y_{v,air}}{1 - Y_{v,surf}} \tag{6}$$

In the convective flux term, *Nu* is the Nusselt number, κ_{air} is the constant thermal conductivity of the gas mixture, and T_{air} is the temperature condition surrounding the droplet. The term C_T represents the Knudsen correlation for non-continuum effects, which is negligible for the sizes considered here ($C_T = 1.0$). Both T_d and T_{air} are variable, and determined by Eqs. (1) and (3), respectively. Due to the small droplet size and associated small particle Reynolds number, the Nusselt number is defined as Nu = 2.0, from the correlation of Clift et al. (1978). For the mass flux expression, Eq. (6), *Sh* is the non-dimensional Sherwood number (also equal to 2.0), $\tilde{D}_v$ is the binary diffusion coefficient of water vapor in air, and $Y_{v,surf}$ is the water vapor mass fraction at the surface of the droplets. This expression includes the effect of droplet evaporation on the evaporation rate, which is referred to as the blowing velocity (Longest and Kleinstreuer 2005). In Eq. (6), C_M is the mass Knudsen number correction, which is equivalent to one as with C_T.

Flux values at the wall can be expressed as

$$\overline{q}_{wall}=\frac{Nu_{wall}\kappa_{air}}{D_{tube}}(T_{wall}-T_{air}) \tag{7}$$

$$\overline{n}_{wall}=\rho_{air}\frac{Sh_{wall}\tilde{D}_v}{D_{tube}}(Y_{v,wall}-Y_{v,air}) \tag{8}$$

Considering the wall heat flux, Eq. (7), the wall temperature (T_{wall}) is held constant. The geometry is assumed to be cylindrical with a characteristic diameter of D_{tube}. It is expected that a majority of droplet growth will occur in distal lung regions, where the flow can be considered laminar and fully developed. Under these conditions, the wall Nusselt number has a constant value of $Nu_{wall} = 3.66$. Similarly in the mass flux expression, $Y_{v,wall}$ is assumed constant for either dry or wet walls and the Sherwood number is $Sh_{wall} = 3.66$.

Considering variable particle and flow field properties, the densities of the multicomponent droplets are calculated as

$$\rho_d=(m_w+m_{drug}+m_{ex})\left(\frac{\rho_w}{m_w+\frac{m_{drug}\rho_w}{\rho_{drug}}+\frac{m_{ex}\rho_w}{\rho_{ex}}}\right) \tag{9}$$

In this expression, *m* and ρ are the masses and densities of water (*w*), drug, and hygroscopic excipient (*ex*). The binary diffusion coefficient of water vapor used in Eqs. (6) and (8) is calculated from (Vargaftik 1975)

$$\tilde{D}_v=2.16\times10^{-5}\left(\frac{T[K]}{273.15}\right)^{1.8}\quad[\mathrm{m^2/s}] \tag{10}$$

The temperature dependent saturation pressure of water vapor is determined from the Antoine equation (Green 1997)

$$P_{v,sat}=\exp\left(23.196-\frac{3816.44}{T[K]-46.13}\right) \quad [\text{Pa}] \tag{11}$$

which is considered to be more accurate than the Clausius-Clapeyron relation across a broad range of temperatures. Relative humidity is calculated based on the saturation pressure of water vapor as follows

$$RH=\frac{P_v}{P_{v,sat}}=\frac{Y_v\rho_{air}R_vT}{Y_{v,sat}\rho_{air}R_vT}=\frac{Y_v}{Y_{v,sat}} \tag{12}$$

where R_v is the gas constant of water vapor.

The mass fraction of water vapor on the droplet surface is a critical variable, which is significantly influenced by both temperature and solute concentration. For a combination particle of soluble drug and excipient, $Y_{v,surf}$ is calculated as

$$Y_{v,surf}=\frac{SKP_{v,sat}(T_d)}{\rho_{air}R_vT_d} \tag{13}$$

where $P_{v,sat}(T_d)$ is the temperature dependent saturation pressure of water vapor, calculated from Eq. (11). The influence of the Kelvin effect on the droplet surface concentration of water vapor is expressed as

$$K=\exp\left[\frac{4\sigma(T_d)}{2r_d\rho_dR_vT_d}\right] \tag{14}$$

where $\sigma(T_d)$ is the temperature dependent surface tension of the droplet. In Eq. (13), the water activity coefficient, S, describes how dissolved molecules affect the surface concentration of water vapor, i.e., the hygroscopic effect, and can be expressed as

$$S=\left(1+\frac{i_{drug}\chi_{drug}+i_{ex}\chi_{ex}}{\chi_w}\right)^{-1} \tag{15}$$

for a drug and hygroscopic excipient combination particle where χ represents the mole fraction of each component. The *i* coefficients account for the effect of molecular dissociation during dissolution and are sometimes referred to as van't Hoff factors. At high concentrations of drug and excipient, the available water may not be sufficient to dissolve all of the material. In these cases, χ_{drug} and χ_{ex} are replaced by the mole fraction solubility limits of each compound in water. This approach assumes an initial droplet model of a solid core of un-dissolved material surrounded by a layer of liquid with a saturated concentration of each solute. This model persists until there is enough water to fully dissolve the drug and excipient. In either case, the mole fraction of water is calculated as

$$\chi_w = 1 - \chi_{drug} - \chi_{ex} \quad (16)$$

It is noted that Eq. (15) has a form similar to Raoult's law and is valid for materials that may ($i > 1$) or may not ($i = 1$) dissociate upon dissolution. Specifically, Raoult's law provides a linear expression to describe activity coefficients at low solute concentrations, as presented by Finlay (2001). In contrast, the expression used in this study is non-linear and better describes activity coefficient data over a wide range of solute mole fractions. Use of Eq. (15) can be further justified by considering that the mole fractions of drug and excipient do not exceed the solubility limit of the material, which is low for most compounds considered in this study ($\chi_{sat} \leq 0.1$; Table 1). Furthermore, values of the i coefficients in this study are determined based on best fits to experimental data over a range of concentrations. Therefore, the application of Eq. (15) can be viewed as a physically based expression for fitting the experimental data. Finally, high accuracy is required at dilute concentrations, which have the largest impact on the final size achieved by the hygroscopic aerosol.

The resulting set of governing equations describing droplet heat and mass transfer was solved using a variable time-step accuracy-controlled coupled differential equation solver in the numerical package MathCAD 13 (Mathsoft Apps.). Reducing the accuracy control limit by an order of magnitude had a negligible (less than 1%) effect on the final predicted droplet and air phase variables.

Standard Respiratory Exposure Conditions

In this study, a fixed set of respiratory exposure conditions was selected to characterize particle size growth as a function of hygroscopic, particle, and aerosol characteristics. It is expected that a majority of growth during EEG occurs in distal lung regions. As a result, wall temperature and RH conditions were set to constant values of T_{wall} = 37 °C and RH_{wall} = 99.5%. A 2 s inhalation time was selected as a conservative exposure period. The governing equations of droplet heat and mass transfer can be applied within individual branches of the respiratory tract or within a representative geometry with a single characteristic diameter. The latter approach was selected for this study to simplify the calculations and form a well described system. The characteristic dimension was selected based on an airway diameter below which the aerosol spends 80% of its residence time in the lungs. To map residence times, the symmetric airway model of Weibel was considered and scaled to a functional residual capacity of 3.5 L. For an inhalation flow rate of 30 L/min, it was determined that 80% of the residence time occurs below the 19^{th} generation, which has a diameter of 0.4 mm. This airway diameter is also representative of the entire alveolar region of the lungs (Haefeli-Bleuer and Weibel 1988) and was therefore used as the single characteristic airway diameter in the equations.

Cases Evaluated

The model is first validated based on the exposure conditions of the *in vitro* experiments. This study then seeks to determine the effects of hygroscopic, particle, and aerosol properties on EEG for a fixed set of respiratory parameters. Hygroscopic effects are evaluated by considering single component and combination particles of model drugs and hygroscopic excipients. Model drugs considered are AS and BD, which are typically thought to be hygroscopic and non-hygroscopic, respectively, based largely on solubility characteristics in water. For the evaluation of excipients, a representative salt (sodium chloride - NaCl), sugar (mannitol – MN), weak acid (citric acid – CA), and liquid (propylene glycol – PG) were selected. As shown in Table 1, these materials represent a range of molecular weights and solubilities, which are expected to affect the hygroscopicity

of the droplet (cf. Eq. 15). Initially, hygroscopic effects will be assessed for fixed particle ($d_{initial}$ = 900 nm) and aerosol (n_{part} = 3.9 × 10^5 part/cm^3) parameters. Particle engineering and aerosol properties will then be evaluated by modifying the initial diameters, drug and excipient mass fractions, and number concentrations.

RESULTS

Calculation of i Coefficients

Experimental measurements were made in this study to determine the water activity coefficients of AS, CA, and PG. Activity coefficients for NaCl and MN were determined from the studies of Cinkotai (1971) and Ninni (2000), respectively. Budesonide is not considered to be soluble in water, and therefore has no hygroscopic effect during condensational growth. The experimentally determined activity coefficients of all soluble compounds considered are shown in Fig. 2 as a function of the soluble mass fraction of solute (mf_s) in water up to the saturation limit (Table 1). Two panels are used based on the presence of moderately soluble (AS, MN, and NaCl) and highly soluble (CA and PG) compounds. In order to represent the hygroscopic effect of molecular dissociation with a single coefficient, curve fits to the experimental data were based on Eq. (15) for a single component solution. The optimal value of *i* providing the best fit to the experimental data was calculated using a minimization routine. For compounds with high saturated mass fractions in water (CA and PG from Table 1), a limit of $mf_s < 0.3$ was used for evaluating the *i* coefficients. This limit was used to ensure accuracy of the *i*-values for dilute droplets, which is needed to ensure accurate estimates of final droplet size. The resulting curve fits are shown in Fig. 2 and calculated *i* coefficient values are reported in Table 1. It is noted that the form of the activity coefficient correlation proposed by Hinds (1999) and translated to this study (Eq. 15), results in *i* coefficients that are slightly higher than with Raoult's law in the form reported by Finlay (2001). For example, the best fit for the NaCl data through mf_s = 0.3 using Eq. (15) resulted in a coefficient of i_{NaCl} = 2.1. In contrast, the Raoult's law form of the equation results in i_{NaCl} = 1.9. As a result, care should be taken to ensure that the *i* coefficients determined in this study are used with the appropriate form of the activity coefficient expression, i.e., Eq. (15).

Model Validation

For the *in vitro* system, experimental measurements of initial and final aerosol sizes are provided in Table 2. The initial mass median aerodynamic diameter (MMAD) was measured at the inlet to the growth zone, as shown in Fig. 1. Vapor condensation on the wall of the drying tube was not observed near the connection to the growth tube, indicating that the aerosol was fully dried. The resulting initial densities for dry particles are shown in Table 2. These density values were then used to calculate the initial geometric size of the particles (d_{geo}). Reported final geometric diameters are based on the measured MMADs and the assumption that the droplet density is $\rho_d \approx 1000$ kg/m^3 at the outlet of the growth tube. The aerosol growth ratio of final to initial size (d/d_o) was then based on the geometric diameters. Standard deviations of the experimental measurements are provided in parentheses based on a minimum of four experimental replicates (Table 2). Representative geometric standard deviations for the AS+NaCl and BD+NaCl combination particles were 1.45 and 1.57, respectively, which indicate a low degree of polydispersity compared with other pharmaceutical aerosols. Experimental measurements of the flow field conditions indicate an average temperature and RH of 28 °C and 99% at the inlet to the growth zone (Fig. 1). This temperature is greater than the ambient and humidified air inlet temperatures due to the heat introduced from the CAG.

For numerical simulation of the *in vitro* system, the measured inlet conditions were applied in conjunction with T_{wall} = 24 °C, RH_{wall} = 100% and a particle residence time of 0.2 s. Comparisons of the *in vitro* experimental results and numerical predictions of the final geometric size and geometric diameter ratio (d/d_0) are shown in Fig. 3. Standard deviations of the *in vitro* measurements (Table 2) are provided as error bars (+/−) on the experimental results. As shown in the figure, the numerical predictions are in good agreement with the experimental results and lie inside the standard deviation bars in most cases. Some error may be introduced due the simulation of a monodisperse aerosol by the model. However, maximum relative errors between the numerical and experimental results are within approximately 10%. Based on this comparison, it appears that the numerical model can accurately predict the growth of both single and multiple component aerosols. The measured *i* coefficients also appear accurate. Moreover, the model accurately predicts the growth of soluble single and multiple component particles (AS and AS + NaCl) and combinations of soluble hygroscopic excipient and insoluble drug compounds (BD + NaCl).

Growth of Single Component Droplets

To better characterize the factors contributing to hygroscopic growth, droplets with a single dissolved species were first considered using the numerical model. As described previously, standard respiratory exposure conditions were assumed with wall conditions of T_{wall} = 37 °C and RH_{wall} = 99.5% for a 2 s exposure period. The droplets had initial diameters of 900 nm, a soluble mass fraction of mf_s = 0.5, and a number concentration of 3.9×10^5 part/cm^3. Hygroscopic properties influencing droplet growth affect the activity coefficient, as shown in Eq. (15), and include the experimentally determined *i* coefficients and the soluble mole fraction of the solute (χ_s). Numerical results of the final to initial size growth ratio of droplet geometric diameter as a function of various growth factors are shown in Fig. 4. In Fig. 4a, the growth ratio demonstrates a clear inverse relationship with the molar mass of the solute (M_s) for both drugs and hygroscopic excipients. From Eq. (15), activity coefficients are lower (and growth is greater) for large values of χ_s. Mole fractions of individual solutes in water are calculated as

$$\chi_s = \frac{\frac{m_s}{M_s}}{\frac{m_s}{M_s}+\frac{m_w}{M_w}} \tag{17}$$

where *m* and *M* represent the mass (kg) and molar mass (kg/kmol) of the solute (*s*) and water (*w*). Clearly, lower M_s results in higher χ_s, which reduces the activity coefficient and increases the particle size growth. However, the solute molar mass does not completely characterize the growth for the respiratory and particle conditions considered. Figure 4b demonstrates that growth can be described for a single component particle and specific initial size by including both i_s and ρ_s in the growth coefficient. Based on Eq. (15), i_s directly impacts the activity coefficient and ρ_s influences the mass term in the mole fraction calculation (Eq. 17). The result is a *"hygroscopic parameter"* ($i_s\rho_s/M_s$) with units of kmol/m^3, which represents a molar density and describes the growth potential of a soluble compound. Figure 4c illustrates that the initial mass fraction of the solute (mf_s) in the droplet influences size increase and causes the growth curves to separate. It is observed that increasing initial mass fractions of the solute from 0.5 to 1.0 increases the growth ratio by a factor of approximately 1.4. This effect of initial drug or excipient loading can be taken into account as a function of the initial solute volume fraction (vf_s). The resulting growth coefficient (GC_1) for a single component droplet is then

$$GC_1 = \frac{i_s \rho_s}{M_s} \mathrm{vf}_s \tag{18}$$

and collapses the data for multiple initial mass fractions into a single well-defined growth curve (Fig. 4d). Here, the initial solute volume faction is calculated as

$$\mathrm{vf}_s = \frac{\frac{\mathrm{mf}_s}{\rho_s}}{\frac{\mathrm{mf}_s}{\rho_s} + \frac{\mathrm{mf}_w}{\rho_w}} \tag{19}$$

The use of vf_s is preferred in defining GC_1 because the base growth coefficient has units of kmol/m^3. In contrast, use of mf_s did not effectively reduce the data to a single curve. For insoluble compounds, like BD, vf_s is taken to be zero. The correlation for single component droplet growth under the defined respiratory and particle conditions is then

$$\frac{d}{d_o} = 1.0 - 0.0254(GC_1) + 0.75(GC_1)^{0.5} \tag{20}$$

This expression is illustrated in Fig. 4d and produced a correlation coefficient of $R^2 = 0.998$, which indicates an excellent representation of the data. It is noted that this correlation is for a single component aerosol with a single initial diameter and number concentration. The influences of multiple components, particle properties, and aerosol characteristics are explored in the following section.

Growth of Multiple Component Particles

For the evaluation of multiple component aerosols, standard respiratory conditions are again assumed for a 2 s exposure period. Particle properties include initial diameters of 500, 900, and 1500 nm with an initial aerosol number concentration of $n_{part} = 3.9 \times 10^5$ part/cm^3. Initial mass loadings of the drug and excipient are $\mathrm{mf}_{\mathrm{drug}} = 0.5$ and $\mathrm{mf}_{\mathrm{ex}} = 0.5$ resulting in no initial water in the particle. Predicted growth ratios for AS and BD combined with each excipient considered, and evaluated as pure drug aerosols, are displayed in Fig. 5. In Fig. 5a, growth ratios are plotted vs. the hygroscopic parameter evaluated for the excipient. At each growth coefficient value, the three initial particle diameters result in slightly different growth ratios due to two-way coupling effects and potential Kelvin effects (for the 500 nm aerosol). Furthermore, differences in hygroscopicity between AS and BD result in two different sets of curves with higher growth ratios for AS. To account for hygroscopic effects of both the excipient (*ex*) and drug, a growth coefficient for combination particles can be formulated as

$$GC_2 = \frac{i_{ex} \rho_{ex}}{M_{ex}} \mathrm{vf}_{ex} + \frac{i_{drug} \rho_{drug}}{M_{drug}} \mathrm{vf}_{drug} \tag{21}$$

Here vf represents the initial soluble volume fraction of the excipient and drug. For insoluble compounds like BD, $\mathrm{vf}_{\mathrm{drug}}$ is set to zero. For all other compounds consider in this study, no limit on the volume fraction is required. As shown in Fig. 5, application of this coefficient collapses the data to an approximate single curve. The resulting correlation for combination

particle growth over a range of initial sizes (500 – 1500 nm) and the specified respiratory and particle conditions is

$$\frac{d}{d_o}=1.0+0.60(GC_2)^{0.5} \tag{22}$$

This correlation provides a good fit to the numerical data (Fig 5b) and has a correlation coefficient of $R^2 = 0.983$. However, some variability is observed for the higher growth ratios as a result of the initial aerosol size.

Effect of Initial Excipient and Drug Loading

The correlation developed above for combination particles (Eq. 22) was based on a single initial excipient and drug loading ratio of mf_{ex}:mf_{drug} = 50:50. However, the GC_2 relation contains the initial volume fraction (vf), which should account for initial mass fraction loadings. To test if Eq. (22) works for multiple particle conditions, initial mf_{ex}:mf_{drug} loading ratios of 50:50 and 25:75 were considered. Drug and excipient compounds included both model drugs and each hygroscopic excipient considered. Predicted growth ratios for these multiple initial loadings are shown in Fig. 6 compared with the developed combination particle correlation (Eq. 22). As shown in the figure, the correlation provides an excellent representation of multiple initial drug and excipient loadings. Furthermore, it is observed that reducing the excipient mass fraction from 0.5 to 0.25 produces a relatively small reduction in the final growth ratio.

Effect of Initial Particle Diameter

The combination particle correlation appears to provide a good estimate of growth for the conditions considered. However, for higher growth ratios ($d/d_o > 3$ and $GC_2 > 10$), the initial aerosol size causes some variability in the data. This effect arises because of two-way coupling. As the aerosol grows larger, more water vapor is required to produce a size change and the amount of water vapor in the air limits the growth for a set exposure time. To address the effect of initial size, a correlation for unobstructed growth is first developed. The growth coefficient is then adjusted to account for both initial particle size and aerosol number concentration.

Unobstructed aerosol growth was considered for standard respiratory exposure conditions with no limit on the exposure time and without two-way coupling (i.e., approximately zero aerosol number concentration). The Kelvin effect was also neglected. As a result, all initial diameters produced the same growth ratio. The correlation representing this unobstructed growth is defined as

$$\frac{d}{d_o}=1.0+0.70(GC_2)^{0.5} \tag{23}$$

and illustrated in Fig. 7.

To determine the effect of initial size on growth, standard respiratory conditions were considered for a 2 s exposure period. Particle properties included a mf_{ex}:mf_{drug} loading ratio of 50:50, initial sizes of 500, 900, and 1500 nm, and an aerosol number concentration of $n_{part} = 3.9 \times 10^5$ part/cm^3. Numerical predictions of particle growth ratios for these conditions are shown in Fig. 7a compared with the unobstructed growth correlation. As

expected, the realistic respiratory and particle conditions reduce growth ratios from the unobstructed case, and this reduction is greater for larger initial sizes and larger growth values.

To fit the realistic numerical growth data to Eq. (23), effects of initial size were incorporated into the growth coefficient as

$$GC_3 = GC_2 - \Delta_1 \tag{24}$$

where GC_2 is defined in Eq. (21). The Δ coefficient represents the decrease in the growth coefficient value arising from initial size effects. Best fits of the numerical data to Eq. (23) resulted in the following Δ values:

if $GC_2 \geq 10$

$$\Delta_1 = 0.0336 d_0 (GC_2)^{1.62} \tag{25a}$$

if $GC_2 < 10$

$$\Delta_1 = \frac{GC_2}{0.125(GC_2)+6.7} \tag{25b}$$

where the diameter term d_o is the initial particle or droplet geometric diameter in micrometers (μm). The first Δ relation (Eq. 25a) indicates that both initial diameter and the amount of growth (represented by GC_2), influence the final particle size. For smaller GC_2 values (< 10), Eq. (25b) indicates that the amount of growth is the primary factor in limiting the final size. The resulting growth coefficient fits the numerical data very well (Fig. 7b). Therefore, the combination of the unobstructed growth correlation (Eq. 23) with GC_3 (Eq. 24) can be used to accurately predict growth for multiple initial sizes, components, and loading ratios with an approximate number concentration of 3.9×10^5 part/cm^3.

Effect of Number Concentration

The previous results are based on a single aerosol number concentration of $n_{part} = 3.9 \times 10^5$ part/cm^3. This value is representative of the CAG delivering 10 mg/s of a drug solution. However, other deliver devices may produce different aerosol number concentrations when combined with the patent's inhalation flow rate. To consider the effects of aerosol number concentration, values of 3.9×10^5, 5.0×10^6, and 1.0×10^7 part/cm^3 were evaluated, which span a range of approximately two orders of magnitude. As before, standard respiratory exposure conditions were assumed for initial diameters of 500, 900, and 1500 nm and 50:50 excipient to drug initial mass ratio. Numerical predictions of growth for these different number concentrations are compared with Eq. (23) for growth coefficients GC_2 and GC_3 in Figs. 8a and b, respectively. Aerosol number concentration is observed to reduce the growth ratio due to increasing two-way coupling effects. However, the GC_3 relation provides a reasonable approximation to growth through a concentration of 1.0×10^7 part/cm^3. The data for various number concentrations is fit very effectively using a new growth coefficient

$$GC_4 = GC_2 - \Delta_2 \tag{26}$$

where for all values of GC_2, the effects of both initial particle size and number concentration can be approximated as

$$\Delta_2 = 0.0443\, d_o (GC_2)^{\sqrt{2}} \left(\frac{n_{part}}{1 \times 10^5} \right)^{0.154} \tag{27}$$

In this expression, the initial aerosol diameter d_o is again entered in micrometers and the aerosol number concentration has units of particles/cm^3. Figure 8c illustrates that the GC_4 relation combined with Eq. (23) fits the growth data very well across a range of drugs, excipients, initial sizes, loadings, and number concentrations.

DISCUSSION

The numerical model developed in this study was found to accurately predict the size increase of single and multiple component pharmaceutical aerosols in comparison with *in vitro* experiments. For a fixed set of respiratory exposure conditions, the model was then used to explore the effects of hygroscopic characteristics, particle engineering parameters, and aerosol properties on particle size growth. Considering a single component aerosol, molar density of the solute ($i_s\rho_s/M_s$) was identified as a hygroscopic parameter that described the growth potential of the compound. Combination of this hygroscopic parameter with the volume fraction of the solute produced a growth coefficient (GC_1) that collapsed the single component growth data to a well defined curve. For combination particles, a sum of growth coefficients for the drug and excipient components (GC_2) was shown to correlate the growth data very well over a range of drugs, hygroscopic excipients, and initial particle sizes. The resulting correlation was also found to be valid for different initial drug to excipient mass loading ratios. For an initial mf_{ex}:mf_{drug} ratio of 50:50, the final to initial diameter ratios ranged from approximately 2.3–4.6 for AS (a soluble hygroscopic drug) and from 2.1–4.2 for BD (an insoluble non-hygroscopic drug) over the spectrum of excipients that were considered. More detailed growth coefficients were then developed to better account for the effects of initial size and aerosol number concentration, which can both limit growth through two-way coupling. The growth coefficient presented in Eq. (26), i.e. GC_4, was shown to effectively predict aerosol size increase in the respiratory airways for a range of drugs, hygroscopic excipients, initial diameters, particle loading conditions, and aerosol number concentrations. It was observed that even at the maximum aerosol number concentration considered ($n_{part} = 1\times10^7$ part/cm^3), Eq. (23) in combination with GC_4 predicted aerosol size increases up to 4.5 for the drugs and excipients considered in this study.

An interesting finding of this study was the correlation between the initial mole fraction (i.e., hygroscopic parameter) of the solute in the particle or droplet and the diameter growth ratio. The product of the hygroscopic parameter ($i_s\rho_s/M_s$) and volume fraction of the solute was then the basis for all droplet growth coefficients in this study. Based on these results, $i_s\rho_s/M_s$ values can be used to determine the hygroscopic growth characteristics of soluble drugs and excipients. Compounds with the greatest hygroscopic potential, and therefore good candidates for EEG delivery, have high i coefficients and low molecular weights (M_s). High density also increases the $i_s\rho_s/M_s$ parameter; however, high density may reduce the excipient volume fraction depending on the density of the drug. Table 1 provides values of $i_s\rho_s/M_s$ for all compounds considered in this study. The hygroscopic excipients are observed to all have $i_s\rho_s/M_s$ values at least double the value of AS, which makes them good candidates for EEG delivery. NaCl is by far the most hygroscopic compound considered, followed by CA and PG. The range of hygroscopic potential reported in Table 1 gives flexibility to drug

formulators in order to engineer specific size increases and rates of increase to target deposition within different regions of the lungs. Furthermore, definition of the hygroscopic parameter provides valuable insight regarding the expected performance of other potential excipients and drugs that may be used for EEG delivery.

In this study, a range of correlations is provided for determining the hygroscopic growth of single and multicomponent particles or droplets in the airways for typical respiratory conditions. The simpler correlations are most valid for a single initial size and number concentration where two-way coupled effects are limited. More advanced correlations are then required to account for the effects of the initial size, the initial concentration, and two-way coupling. For targeted aerosol drug delivery to the lungs, whole-lung 1-D models (Asgharian et al. 2001) or more detailed CFD models (Xi et al. 2008) of deposition can be used to determine the desired initial and final sizes of the aerosol. For example, negligible mouth-throat deposition typically occurs for 900 nm particles (Hindle and Longest 2010) and full lung retention can occur for 3.0 μm droplets (Stahlhofen et al. 1989) resulting in a final to initial diameter ratio of 3.3. The correlations provided in this study can then be used to engineer the particles to achieve the desired size increase and maximize the drug payload of the aerosol. For a quick calculation of expected size increase at typical EEG initial aerosols sizes (500–900 nm) and number concentrations ($n_{part} \approx 4 \times 10^5$ part/cm^3), Eq. (22) in conjunction with GC_2 provides a simple relationship. Comparison between Eq. (22) and the unobstructed growth correlation Eq. (23) with GC_2 indicates that the former expression reduces the final diameter ratio by a maximum of 10% due to two-way coupling effects. For more precise calculations that effectively collapse the data to a single curve by accounting for both initial size and number concentration, Eq. (23) is recommended with the use of GC_4. Based on the implementation of three initial sizes (500–900 nm) and three aerosol number concentrations ($3.9\times10^5 - 1.0\times10^7$ part/cm^3), GC_4 can be applied to both larger initial particle sizes and number concentrations than those considered in this study. Lower number concentrations are not expected to have a significant effect on growth and can therefore also be analyzed with the correlations developed in this study. However, caution should be exercised when applying the correlation to initial sizes less than 500 nm as Kelvin effects were included in the model but were not largely present over the size range considered. These correlations can also be used to describe the growth of conventional pharmaceutical aerosols composed of single and multiple components. Single component aerosols can be analyzed using either Eq. (20) or the more advanced relations with only one volume fraction retained. Moreover, aerosols with more than two components can be analyzed with the developed correlations by including additional terms in the GC_2 relations as follows

$$GC_2 = \sum_{j=1}^{N} \frac{i_j \rho_j}{M_j} \mathrm{vf}_j \tag{28}$$

where the summation is performed over the total number of compounds (N). This expression can then be used in Eqs. (26) and (27) to define a GC_4 parameter for more than two compounds, which accounts for two-way coupling effects.

The utility of the developed correlations is illustrated by considering an example in which insulin is to be delivered using the EEG approach. Proposed values for initial and final diameters are 900 nm and 3 μm, which are suitable for producing minimal mouth-throat deposition and nearly complete retention in the alveolar region. As a conservative estimate, insulin is assumed insoluble and NaCl is the hygroscopic excipient selected. It is also assumed that the delivery device produces an aerosol number concentration of 1×10^6 part/

cm^3 (1×10^{12} part/m^3). To engineer the particles for optimal EEG delivery, the minimum mass loading of the hygroscopic excipient to produce the desired size change in the aerosol needs to be determined. Using the most detailed correlation developed, Fig. 8c or Eq. (23) indicated that the necessary value of GC_4 is 10.8 to achieve a growth ratio of 3.33. Solving Eq. (26) for a known GC_4 value then indicates an initial NaCl volume fraction of 0.165, which translates to an initial excipient mass fraction of 0.30. Therefore, a relatively small amount of the hygroscopic excipient, NaCl, is required to produce the required growth to 3 μm for typical respiratory conditions with a non-hygroscopic drug and achieve full lung retention of the aerosol. Moreover, use of the developed correlation ensures that each particle delivers the maximum amount of drug and minimum amount of excipient possible for the prescribed aerosol growth.

Two primary assumptions made in the experiments were that the aerosol was fully dry at the inlet of the growth tube and that no growth occurred in the impactor. Dry powder particles were recovered on a single stage impaction plate for analysis of drug content:excipient ratio and the measured ratio was observed to agree with the nominal drug:excipient ratio. Considering this observation and that the walls of the growth tube remained dry near the exit, it is reasonable to conclude that the aerosol consisted of dry or nearly dry particles prior to condensational growth. Furthermore, some diameter change is expected during aerosol sizing that is not captured in the model arising from (i) a finite residence time and (ii) pressure drops at different stages in the impactor. If these factors were significant, then a bias toward larger experimental sizes and numerical under-predictions of the data would be expected in Fig. 3. However, the numerical model is observed to be within the standard deviation range of the experiments in most cases and does not indicate a bias toward over- or under-prediction of the *in vitro* data. As a result, effects of both the initially dry aerosol assumption and size change in the impactor are expected to be minor in this study.

Limitations of the developed models and correlations include assumptions made in estimating the respiratory conditions, hygroscopic characteristics, particle model, and aerosol properties. A fixed set of respiratory conditions was assumed in this study as a baseline to allow for an assessment of multiple other parameters on growth. Clearly, the correlations developed are dependent on a 2 s exposure period and wall conditions of 37 °C and 99.5% RH. These conditions may differ as a function of breathing patterns or disease state. However, airway wall conditions in the deep lung are thought to be relatively stable. A characteristic airway diameter was used based on the assumption that a majority of residence time and therefore a majority of growth occurs in the lower airways. However, hygroscopic growth is also known to occur in the upper conducting airways (Ferron et al. 1989; Zhang et al. 2006a). As a result, the consideration of only lower airway conditions and neglecting growth in the upper airways provides a conservative estimate of the size increase that can be achieved. Furthermore, Sherwood and Nusselt numbers in the bifurcating and alveolar airways will be larger than the values implemented for straight and smooth walled tubes, which will also increase the rate of growth *in vivo*. In the validation study, capturing the time dependent wall temperature changes associated with the delivery of a 2 s aerosol bolus will require more advanced simulations. Considering hygroscopic conditions, a non-linear function that provides higher accuracy than Raoult's law across a range of solute concentrations was applied. Values of the *i* coefficients were experimentally determined through the saturation limit in most cases. Still, some differences were observed between the predicted and measured values of activity coefficients at higher mass fractions. A more complex expression of activity coefficients could easily be used to better fit the experimental data, as with Cinkotai (1971). However, use of a more advanced correlation would significantly increase the complexity of the hygroscopic parameter ($i_s\rho_s/M_s$) and growth coefficients making the developed growth expressions cumbersome and difficult to apply. In determining solubility, interactions between the drug and excipient were not considered.

Furthermore, the effect of one compound on the activity coefficient of another was excluded. These interactions are expected to increase the hygroscopic growth potential of real aerosols. A monodisperse particle distribution was assumed for each size considered in the numerical model. The aerosol was also assumed to have a constant number concentration. As the aerosol penetrates into the airway bifurcations and alveolar region, mixing with existing air and some deposition are expected, which will reduce the number concentration. Aerosol coagulation, which may occur at some of the higher number concentrations considered, was also neglected. The assumption of a constant concentration is again conservative because reduced concentrations will increase the growth potential. Considering these assumptions together, condensational growth *in vivo* is expected to be greater than predicted with the developed models and correlations. Growth predictions did agree well with the simple *in vitro* model with no clear indication of over or under prediction. As a result, the model developed here provides a baseline estimate for further *in vitro*, numerical, and *in vivo* testing of the EEG concept.

In conclusion, the model and correlations developed in this study can be used to effectively describe particle properties that achieve a specified amount of size increase during EEG delivery under standard respiratory drug delivery conditions. These correlations can also be used to predict the size increase of conventional single and multicomponent aerosol in the respiratory airways. Considering EEG delivery, significant size increases were observed for a range of hygroscopic excipients combined with both hygroscopic and non-hygroscopic drugs. These size increases are expected to be sufficient to allow for minimal mouth-throat deposition and nearly full lung retention. The developed correlations can also be applied to screen the performance of other excipients and drugs not considered in the base set of sample compounds. Interesting, large diameter growth ratios were achieved at excipient mass loadings of 50% and below and at realistic aerosol number concentrations. It was illustrated that the developed correlations can be used to maximize drug content and minimize the necessary hygroscopic excipient of engineered particles to achieve a specific size increase. Future studies are needed to validation model predictions at longer residence times, consider variable lung conditions, determine aerosol size increase and deposition in more realistic airway models using CFD simulations and experiments, and assess model predictions compared with *in vivo* data.

Acknowledgments

This study was supported by Award Number R21 HL104319-01 from the National Heart, Lung, And Blood Institute. The content is solely the responsibility of the authors and does not necessarily represent the official views of the National Heart, Lung, And Blood Institute or the National Institutes of Health.

References

Asgharian B, Hofmann W, Bergmann R. Particle deposition in a multiple-path model of the human lung. Aerosol Science and Technology. 2001; 34:332–339.

Borgstrom L, Olsson B, Thorsson L. Degree of throat deposition can explain the variability in lung deposition of inhaled drugs. Journal of Aerosol Medicine. 2006; 19:473–483. [PubMed: 17196076]

Broday DM, Georgopoulous G. Growth and deposition of hygroscopic particulate matter in the human lung. Aerosol Science and Technology. 2001; 34:144–159.

Byron PR, Delvadia RR, Longest PW, Hindle M. Stepping into the trachea with realistic physical models: Uncertainties in regional drug deposition from powder inhalers. Respiratory Drug Delivery. 2010; 1:215–224.

Cheng YS, Fu CS, Yazzie D, Zhou Y. Respiratory deposition patterns of salbutamol pMDI with CFC and HFA-134a formulations in a human airway replica. Journal of Aerosol Medicine. 2001; 14(2): 255–266. [PubMed: 11681657]

Cinkotai FF. The behavior of sodium chloride particles in moist air. Journal of Aerosol Science. 1971; 2:325–329.

Clift, R.; Grace, JR.; Weber, ME. Bubbles, Drops, and Particles. Academic Press; New York: 1978.

Ferron GA, Oberdorster G, Hennenberg R. Estimation of the deposition of aerosolised drugs in the human respiratory tract due to hygroscopic growth. Journal of Aerosol Medicine. 1989; 2:271.

Finlay WH. Estimating the type of hygroscopic behavior exhibited by aqueous droplets. Journal of Aerosol Medicine. 1998; 11(4):221–229. [PubMed: 10346665]

Finlay, WH. The Mechanics of Inhaled Pharmaceutical Aerosols. Academic Press; San Diego: 2001.

Finlay WH, Stapleton KW. The effect on regional lung deposition of coupled heat and mass-transfer between hygroscopic droplets and their surrounding phase. Journal of Aerosol Science. 1995; 26(4):655–670.

Green, DW. Handbook. McGraw-Hill; New York: 1997. Perry's Chemical Engineers'.

Haefeli-Bleuer B, Weibel ER. Morphometry of the human pulmonary acinus. The Anatomical Record. 1988; 220:401–411. [PubMed: 3382030]

Hardaker LEA, Hatley RHM. *In vitro* characterization of the I-neb adaptive aerosol delivery (AAD) system. Aerosol Medicine and Pulmonary Drug Delivery. 2010; 23(S1):S11–S20. [PubMed: 20373905]

Hindle, M.; Byron, PR.; Jashnani, RN.; Howell, TM.; Cox, KA. High efficiency fine particle generation using novel condensation technology. In: Dalby, RN.; Byron, PR.; Farr, SJ., editors. Proceedings of Respiratory Drug Delivery VI. Interpharm Press, Inc; Buffalo Grove, IL: 1998. p. 97-102.

Hindle M, Longest PW. Evaluation of enhanced condensational growth (ECG) for controlled respiratory drug delivery in a mouth-throat and upper tracheobronchial model. Pharmaceutical Research. 2010; 27:1800–1811. [PubMed: 20454837]

Hinds, WC. Aerosol Technology: Properties, Behavior, and Measurement of Airborne Particles. John Wiley and Sons; New York: 1999.

Leach CL, Davidson PJ, Bouhuys A. Improved airway targeting with the CFC-free HFA-beclomethasone metered-dose inhaler compared with CFC-beclomethasone. European Respiratory Journal. 1998; 12:1346–1353. [PubMed: 9877489]

Longest PW, Hindle M. Evaluation of the Respimat Soft Mist inhaler using a concurrent CFD and *in vitro* approach. Journal of Aerosol Medicine and Pulmonary Drug Delivery. 2009a; 22(2):99–112.

Longest, PW.; Hindle, M. Excipient enhanced growth (EEG) of nanoparticle aerosols to enable improved pulmonary targeting and retention, Provisional Patent Application. 2009b.

Longest PW, Hindle M. CFD simulations of enhanced condensational growth (ECG) applied to respiratory drug delivery with comparisons to *in vitro* data. Journal of Aerosol Science. 2010; 41:805–820. [PubMed: 20835406]

Longest PW, Hindle M, Das Choudhuri S, Byron PR. Numerical simulations of capillary aerosol generation: CFD model development and comparisons with experimental data. Aerosol Science and Technology. 2007; 41:952–973.

Longest, PW.; Hindle, M.; Das Choudhuri, S.; Byron, PR. Developing a better understanding of spray system design using a combination of CFD modeling and experiment. In: Dalby, RN.; Byron, PR.; Peart, J.; Suman, JD.; Farr, SJ.; Young, PM., editors. Proceedings of Respiratory Drug Delivery 2008. Davis Healthcare International Publishing; Illinois: 2008a. p. 151-163.

Longest PW, Hindle M, Das Choudhuri S, Xi J. Comparison of ambient and spray aerosol deposition in a standard induction port and more realistic mouth-throat geometry. Journal of Aerosol Science. 2008b; 39:572–591.

Longest PW, Kleinstreuer C. Computational models for simulating multicomponent aerosol evaporation in the upper respiratory airways. Aerosol Science and Technology. 2005; 39:124–138.

Longest PW, McLeskey JT, Hindle M. Characterization of nanoaerosol size change during enhanced condensational growth. Aerosol Science and Technology. 2010; 44:473–483. [PubMed: 20640054]

Longest PW, Xi J. Condensational growth may contribute to the enhanced deposition of cigarette smoke particles in the upper respiratory tract. Aerosol Science and Technology. 2008; 42:579–602.

Newman, S. Respiratory Drug Delivery: Essential Theory and Practice. RDD Online; Richmond: 2009.

Newman SP, Busse WW. Evolution of dry powder inhaler design, formulation, and performance. Respiratory Medicine. 2002; 96:293–304. [PubMed: 12113378]

Nikander K, Prince I, Coughlin S, Warren S, Taylor G. Mode of Breathing-Tidal or slow and deep-through the I-neb adaptive delivery (ADD) system affects lung deposition of 99mTc-DTPA. Journal of Aerosol Medicine. 2010; 23(S1):S37–S43.

Ninni L, Camargo MS, Meirelles AJA. Water activity in polyol systems. J Chem Eng Data. 2000; 45:654–660.

Pitcairn G, Reader S, Pavia D, Newman S. Deposition of corticosteriod aerosol in the human lung by Respimat Soft Mist inhaler compared to deposition by metered dose inhaler or by Turbuhaler dry power inhaler. Journal of Aerosol Medicine. 2005; 18(3):264–272. [PubMed: 16181001]

Robinson R, Yu CP. Theoretical analysis of hygroscopic growth rate of mainstream and sidestream cigarette smoke particles in the human respiratory tract. Aerosol Science and Technology. 1998; 28:21–32.

Stahlhofen W, Rudolf G, James AC. Intercomparison of experimental regional aerosol deposition data. Journal of Aerosol Medicine. 1989; 2(3):285–308.

Vargaftik, NB. Tables on Thermophysical Properties of Liquids and Gases. Hemisphere; Washington, DC: 1975.

Varghese SK, Gangamma S. Particle deposition in human respiratory system: Deposition of concentrated hygroscopic aerosols. Inhalation Toxicology. 2009; 21(7):619–630. [PubMed: 19459776]

Xi J, Longest PW, Martonen TB. Effects of the laryngeal jet on nano- and microparticle transport and deposition in an approximate model of the upper tracheobronchial airways. Journal of Applied Physiology. 2008; 104:1761–1777. [PubMed: 18388247]

Zhang Y, Gilbertson K, Finlay WH. In vivo-*in vitro* comparison of deposition in three mouth-throat models with Qvar and Turbuhaler inhalers. Journal of Aerosol Medicine. 2007; 20(3):227–235. [PubMed: 17894531]

Zhang Z, Kleinstreuer C, Kim CS. Isotonic and hypertonic saline droplet deposition in a human upper airway model. Journal of Aerosol Medicine. 2006a; 19(2):184–198. [PubMed: 16796543]

Zhang Z, Kleinstreuer C, Kim CS. Water vapor transport and its effects on the deposition of hygroscopic droplets in a human upper airway model. Aerosol Science and Technology. 2006b; 40:52–67.

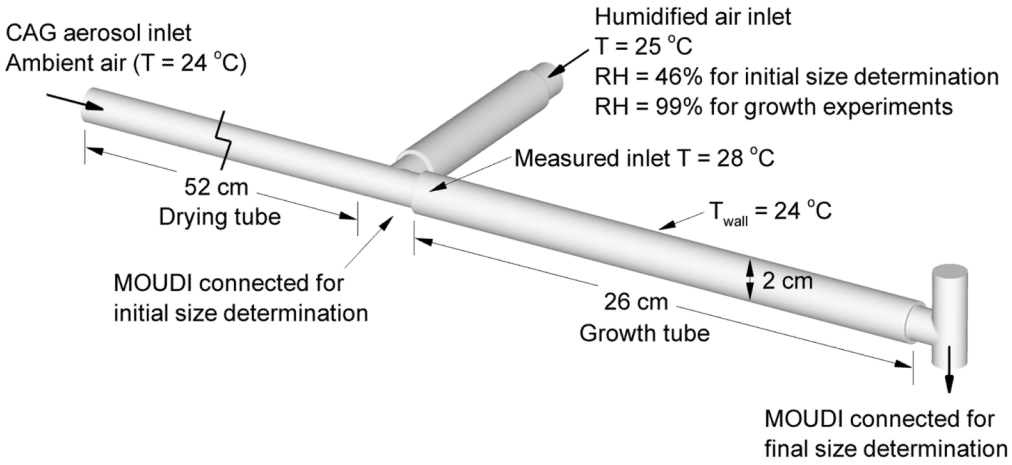

Fig. 1.

Experimental system used to evaluate initial aerosol size and to determine aerosol growth over a short exposure period for comparisons with the numerical model.

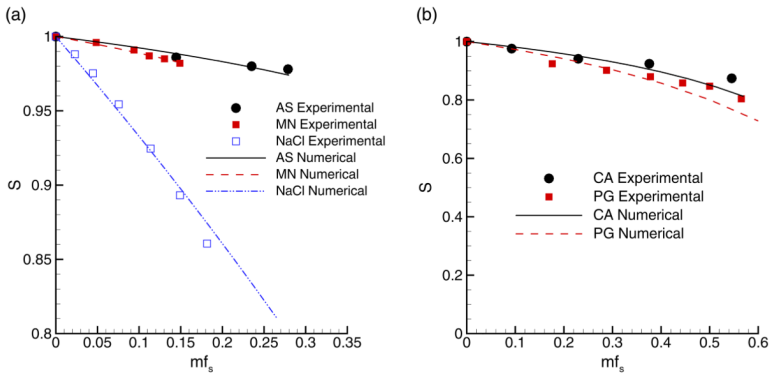

Fig. 2.

Experimental and numerical predictions of activity coefficients (S) over a range of solute mass fractions in water at 25 °C for (a) moderately soluble and (b) highly soluble compounds.

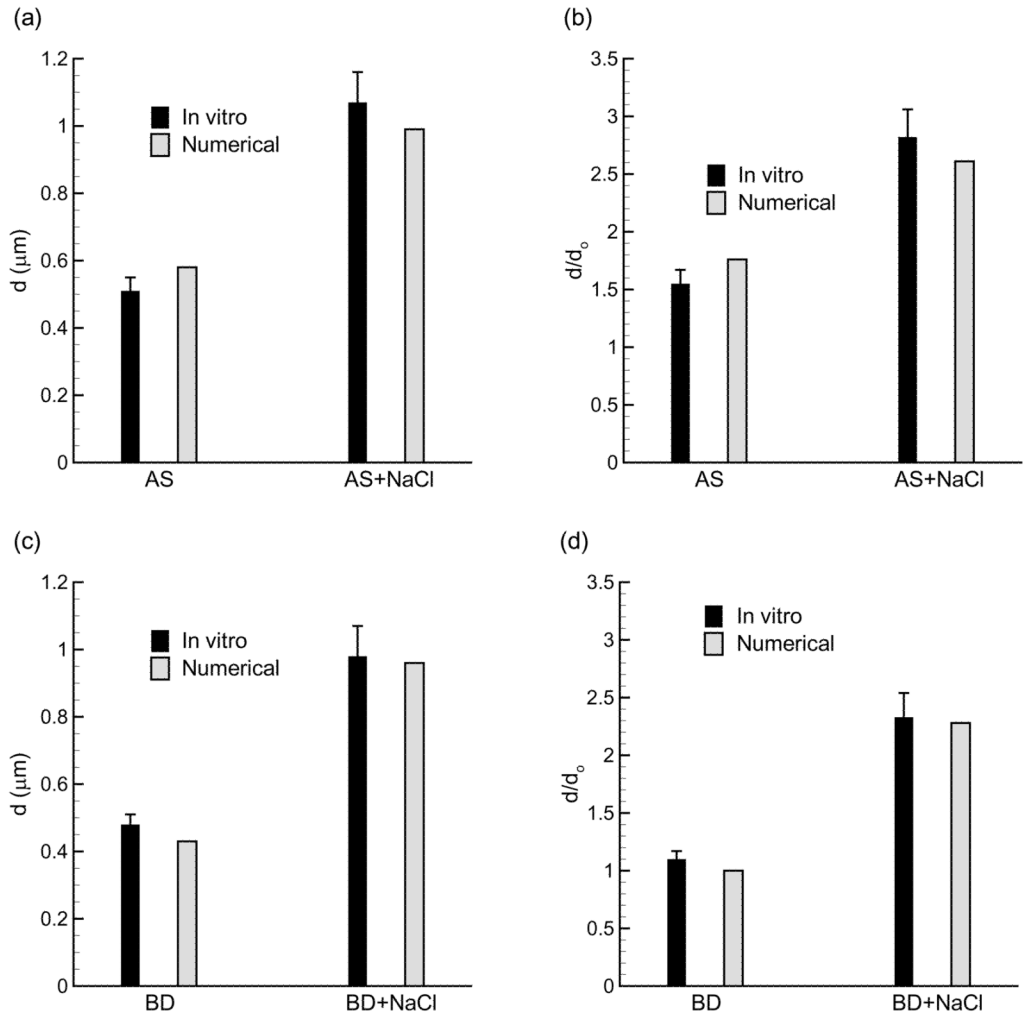

Fig. 3.

Final geometric diameter and diameter growth ratio based on *in vitro* results and numerical predictions of (a & b) AS and AS+NaCl combination particles and (c & d) BD and BD +NaCl combination particles. Panels (a) and (c) report the final geometric diameter whereas panels (b) and (d) illustrate the diameter growth ratio. In all cases, the numerical predictions provide a good estimate to the *in vitro* results for conditions consistent with the experimental system.

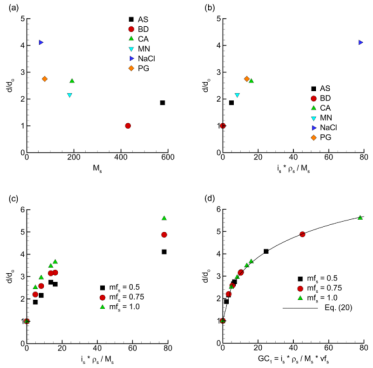

Fig. 4.

Geometric diameter growth ratio for single component aerosols (a) as a function of molecular weight, (b) as a function of the hygroscopic parameter, (c) for different initial solute mass fractions (mf_s) in water, and (d) as a function of growth coefficient GC_1.

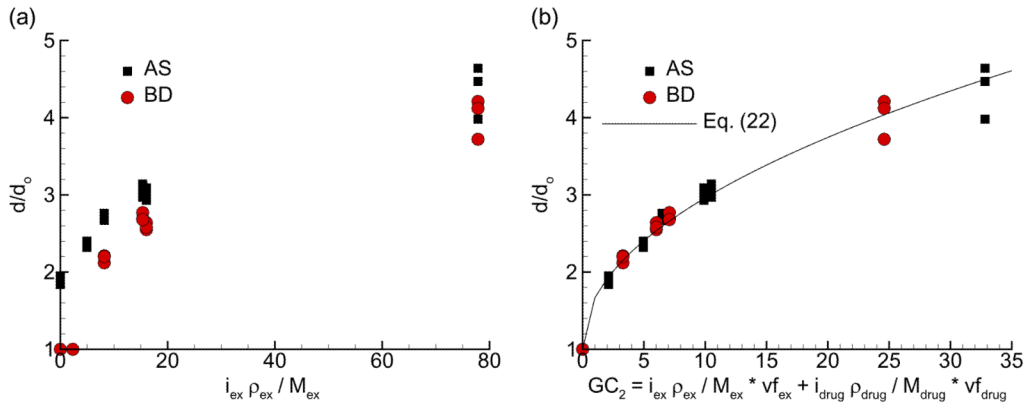

Fig. 5.

Diameter growth ratios for AS and BD combination particles with each hygroscopic excipient based on (a) the hygroscopic growth parameter and (b) GC_2, which accounts for the growth potential of both the excipient and drug. Use of the GC_2 parameter collapses the growth data to an approximate single curve for combination drug and excipient particles.

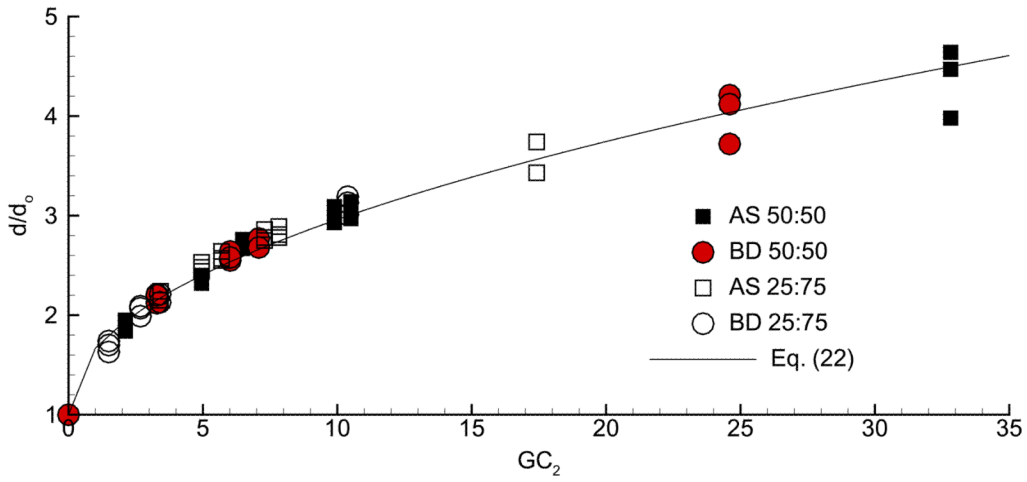

Fig. 6.

Growth ratio as a function of GC_2 for initial mf_{ex}:mf_{drug} particle loadings of 50:50 and 25:75. Based on the use of the GC_2 parameter, the growth correlation represents size increase for multiple initial excipient and drug loadings.

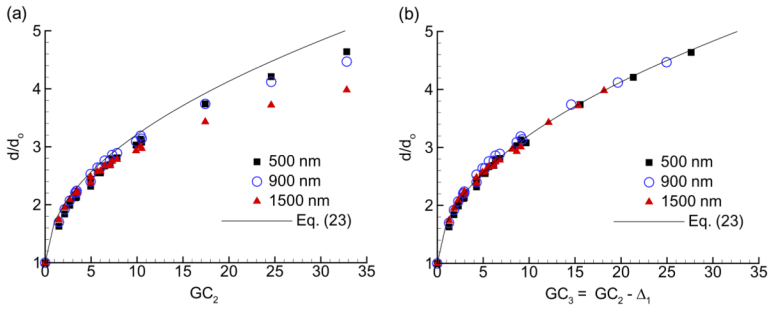

Fig. 7.

Comparison of the correlation for unobstructed aerosol growth with growth data as a function of (a) GC_2 and (b) GC_3 for a range of initial aerosol sizes. Implementation of GC_3 with Eq. (23) fits the growth data very well for all initial aerosols sizes, drugs, and excipients considered.

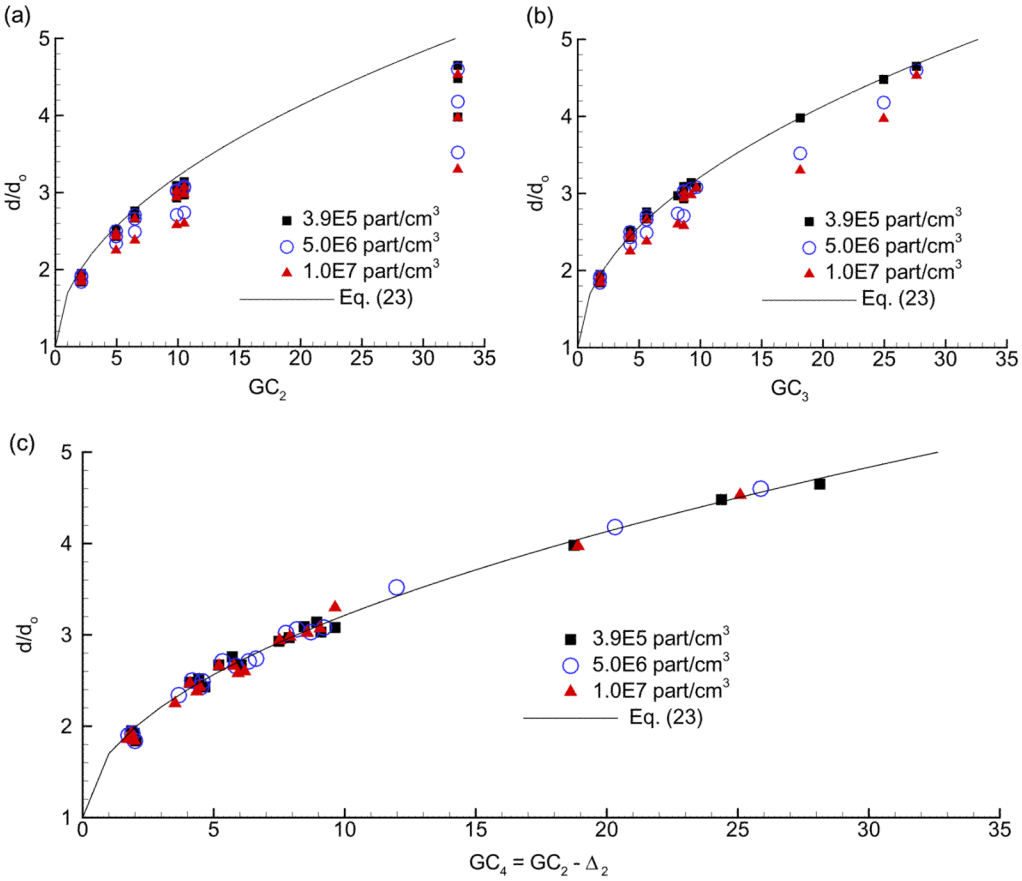

Fig. 8.

Growth ratio over a range of multiple initial sizes (500 – 1500 nm) and aerosol number concentrations (3.9×10^5 – 1.0×10^7 part/cm^3) as a function of (a) GC_2 and (b) GC_3. As aerosol number concentration increases above 3.9×10^5 part/cm^3, use of both GC_2 and GC_3 produces an over prediction of growth due to two-way coupling. In contrast, GC_4 is shown (c) to account for growth across a wide range of drugs, excipients, initial sizes, and number concentrations.

Table 1

Hygroscopic properties of drugs and excipients.

Compound	Density (ρ) kg/m^3	Molar mass (M) kg/kmol	Saturated mass fraction (mf_{sat}) [b]	Saturated mole fraction (χ_{sat}) [c]	Predicted van't Hoff factor (i)	Hygroscopic parameter $i_s\rho_s/M_s$
Water	997.0	18.0	NA	NA	NA	NA
Albuterol sulfate (AS)	1340.	576.7	0.28	0.012	2.1[d]	4.9
Budesonide (BD)	1000.[a]	430.0	Not soluble	Not soluble	NA	NA
Citric acid (CA)	1665.	192.1	0.57	0.11	1.9[d]	16.5
Mannitol (MN)	1489.	182.0	0.15	0.018	1.0[e]	8.2
Sodium Chloride (NaCl)	2165.	58.4	0.265	0.10	2.1[f]	77.9
Propylene glycol (PG)	1036.	76.1	1.00	1.00	1.0[d]	13.6

[a] Approximate value

[b] Mass fraction of compound that can be dissolved in liquid water at 25 °C.

[c] Mole fraction of compound that can be dissolved in liquid water at 25 °C.

[d] Measured in this study.

[e] Based on the measurements of Ninni et al. (2000).

[f] Based on the correlations of Cinkotai (1971).

Table 2

Experimental results of growth for single and multiple component droplets.

Particle components	mf_{drug}	n_{part} (part/cm^3)	ρ_d (kg/m^3)	Initial MMAD (μm)	Initial d_{geo} (μm)	Final d_{geo} (μm)[b]	d/d_o[c]
AS	1.0	4.8×10^5	1340.	0.38 (0.01)[a]	0.33	0.51 (0.04)	1.55 (0.12)
AS + NaCl	0.5	3.9×10^5	1650.	0.49 (0.03)	0.38	1.07 (0.09)	2.82 (0.24)
BD	1.0	6.5×10^5	1000.	0.43 (0.02)	0.43	0.48 (0.03)	1.1 (0.7)
BD + NaCl	0.5	4.7×10^5	1380.	0.49 (0.05)	0.42	0.98 (0.09)	2.33 (0.21)

[a] One standard deviation of each experiment set is shown in parentheses based on a minimum of 4 trials.

[b] Final geometric diameters (d_{geo}) are assumed to be equal to the MMAD.

[c] Calculated based on the ratio of geometric diameters.